Sensitivity of the GFDL Ocean Model to Different Diffusivities for Heat and Salt

ANN E. GARGETT AND GREG HOLLOWAY

Institute of Ocean Sciences, Patricia Bay, Sidney, British Columbia, Canada

(Manuscript received 6 August 1991, in final form 6 December 1991)

ABSTRACT

This work investigates the use of different vertical eddy diffusivity for salt (D_S) and for temperature (D_T) in a coarse-resolution primitive equation ocean model. The diffusivity ratio $d = D_S/D_T$ is taken from a range $0.5 < d < 2.0$ that appears conservative relative to the uncertainty of laboratory, or observational studies, or both of double diffusion and differential diffusion. Conclusions are the following. 1) Major features of the steady-state model solutions are very sensitive to $d \neq 1$. These include the magnitude and direction of the thermohaline circulation, as well as intermediate and deep-water T/S properties and stability. 2) The effects on the model solutions are largely determined by the diffusivity ratio d, rather than the particular choice of the values D_S and D_T by which the value of d is achieved. 3) Effects due to $d \neq 1$ are nonlinear; for example, transport of the meridional thermohaline cell is reduced to 60% of the "normal" ($d = 1$) value when d is only 25% larger than its "normal" value. Implications for climate models and ocean microscale research are discussed.

1. Introduction

This study explores the sensitivity of a coarse-resolution primitive equation ocean model to relaxing the assumption that the vertical turbulent eddy diffusivity for heat D_T is equal to that for salt D_S. We have used the GFDL Ocean Model (Bryan and Cox 1967) because the code has been made widely available and because it is typical of the ocean models being coupled to atmospheric general circulation models (GCMs) for predictive climate studies. Moreover, while increasing computing power may eventually enable us to solve the horizontal parameterization problem by brute force, we will still be faced with the need to parameterize the effects of the yet smaller-scale processes that drive diapycnal fluxes in the ocean. At present, the cumulative effect of small-scale mixing processes is parameterized in coarse-resolution ocean models by a vertical eddy diffusivity D defined by analogy to molecular diffusivity. Thus F_c, the vertical turbulent flux of the scalar variable c, is related to the mean vertical gradient c_z by

$$F_c = -D_c c_z,$$

where D_c is the turbulent eddy diffusivity for the property c. The concept of a turbulent eddy diffusivity has its roots in theories of high Reynolds number homogeneous isotropic turbulence for a medium that is unstratified and a scalar that is passive, that is, does not significantly affect the dynamics of the flow. Leaving aside questions about the conceptual basis for a turbulent eddy diffusivity, its application to the diffusion of heat and salt (both of which affect the density of seawater) in the stratified (anisotropic) interior of the ocean where turbulence is of moderate-to-low Reynolds number is problematical at best. We use it nonetheless; partly through habit and partly because implementing higher-order closures in ocean general circulation models (OGCMs) is equally problematical, given the generally low vertical resolution possible with present computing resources and the absence of strong theoretical, or observational underpinnings, or both for higher-order closures appropriate to the intermittent turbulence that is characteristic of the ocean interior.

That being so, it behooves us to assess the sensitivity of models to various details of eddy diffusivity parameterizations. If the models prove relatively insensitive to what we presently conceive to be a reasonable range of variation in such parameterizations, we gain confidence in the model results. If on the contrary, crucial model variables prove sensitive to particular details of possible parameterizations, we gain some appreciation of which details must be further constrained by observations if models are to develop predictive skill for climate studies.

Bryan (1987) systematically investigated dependence of a low-resolution GFDL model ocean on various parameters, among which was D [A_{HV} in Bryan (1987); assumed equal for T and S]. He found that important aspects of the model results, in particular the vertical scale of the thermocline and the magnitude of the meridional heat transport, were most sensitive to values of D, chosen from a range 0.1–5.0 $cm^2\ s^{-1}$

Corresponding author address: Dr. Ann E. Gargett, Institute of Ocean Sciences, P.O. Box 6000, Sidney, British Columbia, V8L 4B2, Canada.

of constant values that seemed possible, based on a variety of means of estimating D from observations. Briefly, lower values of D led to shallower and sharper thermocline structure, weaker thermohaline circulation, and smaller poleward heat transport. The only one of these large-scale features that is well constrained by observations is the thermocline structure: small values of D, O(0.1–0.3) cm^2 s^{-1}, were required to best approximate the observed character of the main subtropical thermocline. Given the degree of sensitivity to D exhibited by Bryan's model runs, it seemed advisable to examine the effects of further possible refinements to the diffusivity parameterization; first, a suggestion (Gargett 1984) that D was dependent upon stratification, then the possibility that D might not be the same for heat as for salt.

The first question was examined by Cummins et al. (1990, henceforth CHG) using GFDL model configuration and forcing very similar (although not identical) to those used by Bryan (1987). Cummins et al. found that thermocline depth, the sense of the meridional circulation, and poleward heat flux Q_T were all relatively insensitive to the stratification dependence proposed by Gargett (1984):

$$D = a_0 N^{-1}, \tag{1}$$

where $a_0 = 1 \times 10^{-3}$ (cm s^{-1})^2 and $N = (-g\rho_0^{-1}\rho_z)^{1/2}$ is the Brunt–Väisälä frequency. Note that (1) yields upper-ocean diffusivities of order 0.1–0.3 cm^2 s^{-1}, which are comparable to the range of constant D that Bryan (1987) found provided the best fit to thermocline structure. The only significant change produced by the stratification dependence of D was in the deep ocean, where the GFDL model run with constant D has long been known to produce unrealistically homogeneous deep-water properties (Bryan and Sarmiento 1985). Introduction of $D = a_0 N^{-1}$ increased the deep-ocean stratification by an order of magnitude over that produced with constant $D = 0.1$ cm^2 s^{-1}; as well, deep T and S moved toward more realistic (higher) values. Since the meridional heat transport was relatively insensitive to the stratification dependence of D, CHG concluded that this feature of the D parameterization is itself relatively unimportant for the problem of climate modeling (though it may be important for other applications).

This paper examines another fundamental question with respect to an eddy diffusivity parameterization for the ocean, namely, whether the diffusivity used for temperature should equal that for salt. This assumption, almost unquestioned in large-scale ocean modeling, appears increasingly unlikely in light of laboratory and observational evidence of processes such as salt fingering, double diffusive layering, and differential diffusion, all of which result in differential transport of heat and salt in a system where density is a function of both. Let us then define a diffusivity parameter $d \equiv D_S/D_T$ and consider what range of d might be expected due to various differential transport processes known or suspected to occur in the ocean.

Salt fingering (Turner 1973, section 8.2.2) can occur in regions with

$$T_z > 0; \quad S_z > 0; \quad 1 \leqslant R_\rho \equiv \frac{\alpha T_z}{\beta S_z} < \frac{\kappa_T}{\kappa_S},$$

where $\alpha \equiv -\rho_0^{-1}(\partial\rho/\partial T) > 0$ and $\beta \equiv \rho_0^{-1}(\partial\rho/\partial S)$ are, respectively, the coefficients of thermal expansion and haline contraction of seawater, κ_T and κ_S are the molecular diffusivities of temperature and salt, and z is taken positive upward. Salt-finger growth rates and fluxes increase as R_ρ approaches 1, so we expect the process to be active, though possibly intermittent, at values of $R_\rho \sim (1 - 2)$ that are typical of much of the subtropical ocean. Salt fingering is a process that transports salt in the vertical more efficiently than heat (temperature) and can be characterized by a vertical eddy diffusivity for salt,

$$D_S \equiv \frac{-F_S}{S_z},$$

which is larger than that for temperature,

$$D_T \equiv \frac{-F_T}{T_z} = \frac{\gamma_f}{R_\rho} D_S,$$

where $\gamma_f \equiv \alpha F_T/\beta F_S$ is the buoyancy flux ratio. For $R_\rho \approx 1 - 2$ and a value of $\gamma_f \approx 0.6$ (Kunze 1987) to 0.7 (Schmitt 1979), values of $d = R_\rho/\gamma_f$ associated with active salt fingering would be in the range 1.4–3.3.

Double diffusive layering (Turner 1973; section 8.2.1) can occur in regions with

$$T_z < 0; \quad S_z < 0; \quad \frac{\kappa_S}{\kappa_T} < R_\rho \leqslant 1$$

and is a process that transports heat (temperature) more efficiently than salt. For values of $0.5 < R_\rho < 1$, laboratory measurements (Turner 1965) show a regime characterized by constant flux ratio $\gamma_f \approx 6.6$, so diffusive layering in this parameter range can be represented by $d \approx (0.08–0.15)$.

Differential diffusion is much less studied than the two aforementioned double diffusive processes. In two-layer laboratory grid-stirring experiments Turner (1968) found that the transport efficiency of turbulence forced by the grid could depend upon the property (T or S) that was being used to produce the original density difference $\Delta\rho$ between the two layers. For large enough values of overall (layer) Richardson number, the entrainment velocity w_T for the temperature-stratified case was greater than that w_S obtained when salt was used to produce the same $\Delta\rho$. Since entrainment velocity w_c for the scalar c is defined such that

$$w_c \Delta c = F_c = -D_c c_z,$$

the result $w_T > w_S$ can be directly restated as $D_T > D_S$; hence $d < 1$.

Altman and Gargett (1987) carried out measurements in which both T and S contributed to $\Delta\rho$ in the *same* experiment and verified that T and S entrainment velocities were similar to those observed in single component experiments. It is difficult to decide how (or if) these laboratory results may be applied to the ocean, as it is not clear which particular features of the experimental setup are essential to the result of differential diffusion. For the sake of exploration then, let us just consider a value of $d \approx 0.5$ as possible for differential mixing, given the laboratory measurements cited before.

The range $0.5 < d < 2.0$ seems a conservative estimate of a possible range of d values, given the previous discussion of microscale ocean processes that might lead to differential transports of T and S. Moreover, a factor of 2 is a very slight difference, given the accuracy with which we presently estimate diffusive properties from oceanic measurements. In the remainder of this paper we investigate the sensitivity of a simple GFDL box ocean to such apparently slight variation in vertical diffusive parameters.

2. Experiments

This study employs the primitive equation GFDL code developed and distributed by Bryan and Cox (1967) and widely used as an ocean general circulation model for climate studies. The model is physically configured as a simple flat-bottomed box extending 45° in longitude from 0° to 66°N latitude.

Resolution is 3° in both meridional and zonal dimensions, with 15 levels in the vertical: level spacing and depths are found in Table 1. Save in two particulars, the model is identical to that used by CHG, and the reader should refer to this previous study for a detailed description of configuration, resolution, boundary and initial conditions, equation of state, forcing functions, and diffusive parameters other than D, all of which are omitted here for brevity. The two differences are vertical resolution and vertical diffusivity. Cummins et al. report results from model runs with 33 levels in the vertical. These runs initially integrated a model with the 15 vertical levels of Table 1 to steady state. This end state was then interpolated onto a 33-level grid and integrated for an additional 1300 years in the upper ocean (5200 years for the deep ocean, since to accelerate convergence the integration uses the asynchronous time-stepping method of Bryan (1984) with a factor of 4 increase in tracer time step in the deep ocean relative to the upper ocean). The purpose of this increase in vertical resolution was to ensure that there were no aspects of the steady-state solution obtained with 15 vertical levels, which were merely due to problems that can arise when the GFDL code is used with a combination of coarse vertical resolution and small explicit vertical diffusivity (Weaver and Sarachik 1990). Since comparison of the end states of the 15-level and the 33-level integrations revealed only minor quantitative changes, we have carried out the present study with 15 vertical levels. The reduced computational burden associated with fewer levels allows us to perform more numerical experiments, an important consideration when having to explore the two-parameter space that arises when $D_S \neq D_T$.

TABLE 1. Distribution of model levels in the vertical.

Vertical level	Thickness of level (m)	Depth of (T, S) points
1	50	25
2	50	75
3	100	150
4	100	250
5	150	375
6	200	550
7	350	825
8	500	1250
9	500	1750
10	500	2250
11	500	2750
12	500	3250
13	500	3750
14	500	4250
15	500	4750

This brings us to the second and major difference from the work of CHG; namely, that the scalar equations [(8) of CHG] solved for (potential) temperature T and salinity S now involve different vertical diffusivities in addition to different surface forcing functions. For all runs described here,

if $\rho_z > 0$ (static instability),

$$D_S = D_T = 10^4 \text{ cm}^2 \text{ s}^{-1};$$

if $\rho_z < 0$ (static stability), $D_S = \hat{s}D_0$, $D_T = \hat{t}D_0$;

where $D_0 = a_0 N^{-1}$ for all runs except runs 112 and 113, where $D_0 = 0.3 \text{ cm}^2 \text{ s}^{-1}$. Table 2 and Fig. 1 detail the specific combinations of $\hat{s}$, $\hat{t}$, and D_0 that have been used in this study. Reasons for the particular choices will become apparent when results are discussed in the following sections.

3. Results

Most of the numerical experiments reported here use a base diffusivity $D_0 = a_0 N^{-1}$, since CHG showed that this choice provides upper-ocean properties that are comparable with, and deep-ocean properties that are an improvement over, results obtained with a constant diffusivity. For this set (Table 2a), run 120 with $\hat{s} = \hat{t} = 1$ is the standard to which we will compare experiments with $\hat{t} = 1$ and different $\hat{s}$ values (section

TABLE 2. Vertical diffusivity parameters for experiments with constant diffusivity ratio $d \equiv D_S/D_T$. $D_T = \hat{t}D_0$, $D_s = \hat{s}D_0$, hence, $d \equiv \hat{s}/\hat{t}$; $D_{1.5}$ is an equivalent diffusivity for density, evaluated at $R_\rho = 1.5$ (for details, see text, section 5).

Run	d	$\hat{s}$	$\hat{t}$	$D_{1.5}/D_0$
		(a) $D_0 = a_0N^{-1}$:		
138	0.50	0.50	1.00	2.0
120	1.00	1.00	1.00	1.0
134	1.25	1.00	0.80	0.4
131	1.50	1.00	0.66	0.0
139	2.00	1.00	0.50	−0.5
132	2.00	2.00	1.00	−1.0
		(b) $D_0 = 0.3$ cm^{-2} s^{-1}:		
112	1.00	1.00	1.00	1.00
113	2.00	2.00	1.00	−1.00

3a) and experiments with $\hat{s} = 1$ and different $\hat{t}$ values (section 3b). In section 3c, we will briefly examine the results from two runs with constant D_0 (Table 2b) to illustrate that the main qualitative effects observed are not dependent upon having an underlying diffusivity that is dependent upon stratification. All runs have identical surface forcing functions for T, S, and wind stress (Fig. 2). Constancy of wind-stress forcing and momentum diffusion parameters yields the horizontal streamfunction field shown in the center of Fig. 2 for all runs. Heavy lines at 30° latitude and 30° longitude mark standard sections used to compare model results.

a. Experiments with $\hat{t} = 1$, variable $\hat{s}$

Comparison of the standard run 120 ($\hat{t} = 1$, $\hat{s} = d = 1$) with runs 132 ($\hat{t} = 1$, $\hat{s} = d = 2$) and 138 ($\hat{t} = 1$, $\hat{s} = d = 0.5$) quickly reveals that different diffusivities for heat and salt produce major impacts on model results. We illustrate these impacts with a series of diagnostics; the first of which are the sections of meridional and zonal overturning streamfunctions shown in Fig. 3. In the standard run, run 120 (center panels), we see the "normal" thermohaline cell. Driven by high-latitude surface heat loss, water sinks along the northern boundary, spreading equatorward at the deepest model levels, and upwelling at intermediate levels (1–3 km) throughout most of the basin. In the zonal direction, fluid sinks in the eastern part of the basin, upwelling at the western margin. Run 138 with $d = 0.5$ shows similar underlying structure, but very significant (~50%) increase in magnitude. Even more striking is run 132, where the choice $d = 2$ leads to a "normal" thermohaline cell that is only ~25% of that in the standard case and closely confined to the northern boundary, as well as deep circulation beneath the subtropical gyre that is actually reversed in direction. Below ~1-km depth in this model run, the subtropical and equatorial regions of the oceans are isolated from direct (advective) contact with the high-latitude surface heat and salt forcing fields.

One might expect that such dramatic changes in integrated properties like streamfunctions would presage changes in water property distribution, and this is the case. Figure 4 shows the distribution of salinity at two different levels of the model for the three runs. Level 4, with an equivalent depth of 250 m, is in the upper part of the main pycnocline. The salinity distributions in all three runs are similar and consistent with a zonal pattern forced from the surface, deformed by an advective flow with the three-gyre character seen in Fig. 2. (As pointed out previously, this flow field does not vary discernibly for any of the runs discussed here. It is determined by the wind-stress field and the frictional parameters of the model, all of which are kept constant.) Within the equatorial and subtropical gyres of the model, salinity at level 4 is greater (less) than that in the standard run 120 if $d > 1$ ($d < 1$): while in the subpolar gyre this tendency is reversed. Consequently, the meridional salinity gradient is intensified when $d > 1$, and a sharpened property "front" marks the boundary between subtropical and subpolar gyres in run 132.

The lower level 12 shown in Fig. 4b has a nominal depth of 3250 m, deep enough that the advective field is mainly that of the thermohaline cell. Given the dif-

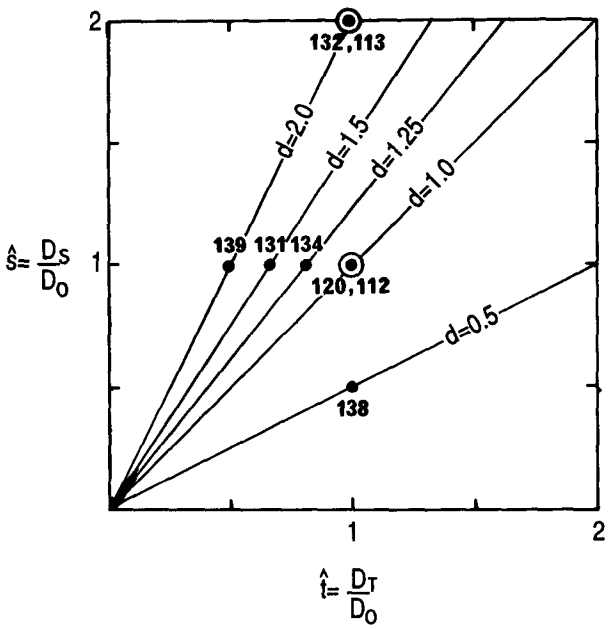

FIG. 1. Location of model runs in the plane of $\hat{t} \equiv D_T/D_0$, $\hat{s} \equiv D_S/D_0$, where D_T and D_S are vertical eddy diffusivities for potential temperature T and salinity S, respectively. Single circles denote runs with $D_0 = a_0N^{-1}$, double circles runs with $D_0 = 0.3$ cm^2 s^{-1}.

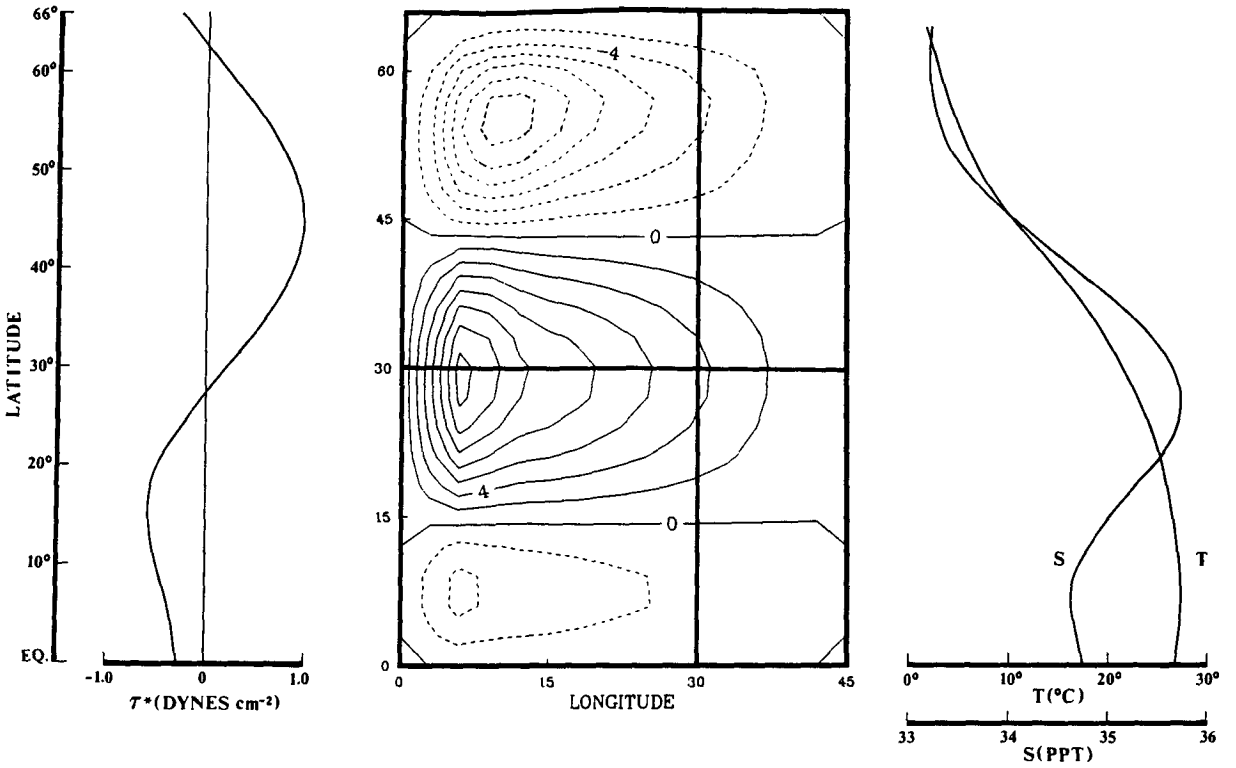

FIG. 2. Meridional variation of wind stress, surface T and S used to force a flat-bottomed box ocean. The resulting horizontal streamfunction (center) is contoured in Sv (1 Sv $\equiv 10^6$ m^3 s^{-1}). Heavy lines at 30° latitude and 30° longitude are the locations of standard sections used to intercompare model runs.

ferences in that cell (seen in Fig. 3), it is not surprising that the deep-water property distributions differ substantially among the three experiments. The pattern of S can be understood as a zonally uniform meridional S gradient, imposed by downward vertical diffusion of salt, deformed by horizontal advection. The horizontal flow field of the standard case, southward along the western boundary with weaker northward return flow over the rest of the basin, produces a northeast–southwest (NE–SW) deformation of isohalines. In run 138, which has a thermohaline cell similar in structure but 50% larger in transport, this advective turning is so much larger that the isohaline trend is now nearly meridional. Run 132 ($d = 2$) is strikingly different, characterized by the nearly zonal isohalines expected if horizontal advection were absent. This is consistent with the meridional circulation shown for the experiment in Fig. 3, where the deep subtropical ocean is seen to be isolated from advective contact with subpolar latitudes. Since it is convection at high latitude that introduces the coldest, freshest water to the deep levels of the model ocean, restriction of the "normal" convective cell to high latitudes at the depth of level 12 combines with increased diffusion of salt into the deep waters [since $D_S(132) = 2D_S(120)$] to produce a subtropical deep water mass that is significantly more salty than the standard case.

Additional information on the spatial distribution of S is shown in the meridional sections of Fig. 5. As pointed out earlier, the upper layers of all experiments have similar patterns, reflecting the nearby surface forcing field and the dominance of advection. Below this, however, both runs 120 and 138 have rather featureless haloclines, with run 138, in particular, showing almost no halocline topography below 1000 m in the meridional direction (as has already been shown at 3250 m from the level 12 map of run 138 in Fig. 4b). By contrast, we see again the strong meridional deep-water gradients of run 132. In this representation, we also see the existence of a subsurface salinity minimum $S_{\min}$ at depths near 1000 m in the subpolar gyre. This feature is strongly reminiscent of the major (deep) salinity minima that extend equatorward from subpolar latitudes in almost all ocean basins (GEOSECS Atlas 1981). (The only exception is the North Atlantic, where the major salt source associated with Mediterranean Water obliterates this feature. Although the present computational domain was chosen roughly comparable to the size of the North Atlantic, the model does not include a Mediterranean salt source; hence, the re-

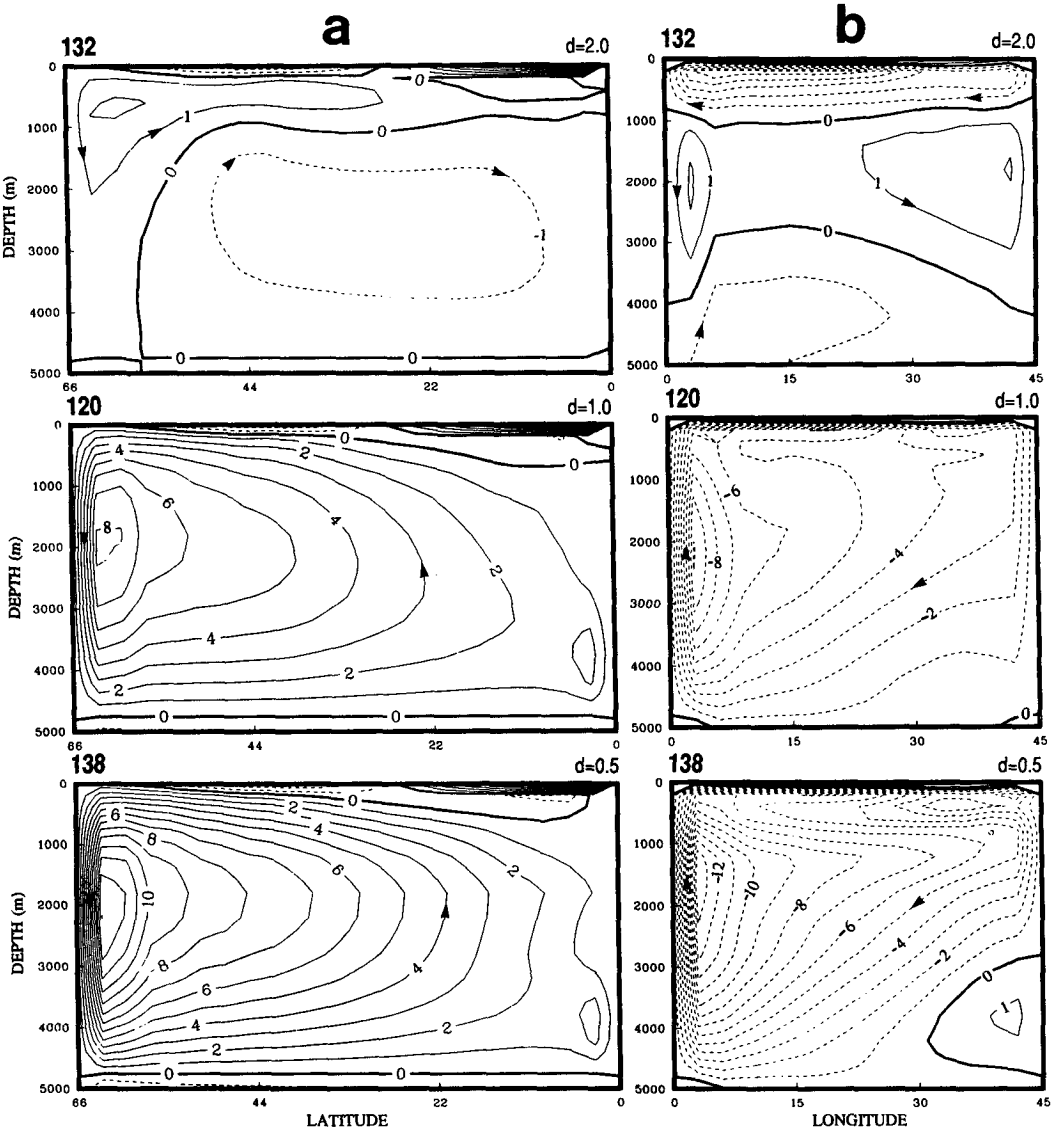

FIG. 3. (a) Meridional and (b) zonal overturning streamfunctions for experiments with $\hat{t} = 1$ and varying d ($\hat{s}$). Upper panels: run 132, $d = 2$; middle panels: "standard" run 120, $d = 1$; lower panels: run 138, $d = 0.5$. Contour interval (c.i.) is 1 Sv; solid contours denote counterclockwise flow.

sulting property distributions should be expected to resemble those of the more "normal" ocean basins.) The deep salinity minima are not reliably reproduced by the GFDL model. Such minima are absent in the box model results of Bryan (1987) and the coupled ocean–atmosphere results of Bryan et al. (1988), but can be caused to appear in an uncoupled model (Bryan 1979) by relaxing to surface salinities much higher than observed near Antarctica (K. Bryan, personal communication). In this work, a salinity minimum is a reliable feature of the model run with $d \gtrsim 1.25$, suggesting that these major features of the ocean T–S structure may depend strongly upon a subtle interplay between advection and microscale diffusion rather than on advection alone.

Changes in water column stratification are also associated with changes in d value, as seen in Fig. 6. The standard run 120 has a relatively featureless field of density gradient, displayed here as $\log(-\rho_z/\rho_0)$. Here, and in all subsequent plots of this field, $(-\rho_z/\rho_0)$ has units of per centimeter: the associated field of N^2 is derived by multiplying by $g = 981$ cm s^{-2}. In run 138, this field is little changed, although a weak middepth stability maximum develops at low latitudes. In run 132 ($d = 2$), deep ocean stability is reduced, particularly along the northern boundary. We will discuss a

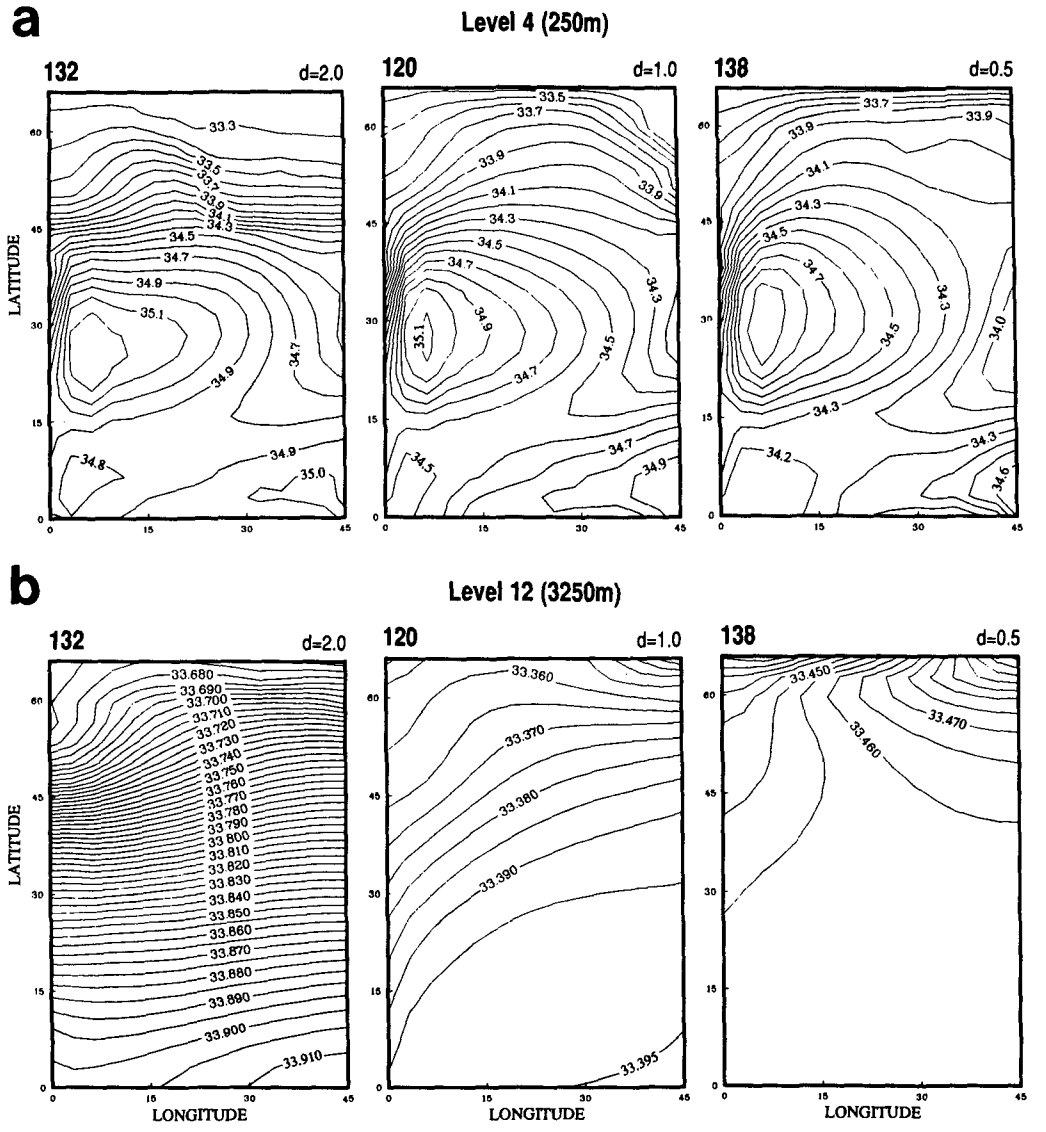

FIG. 4. (a) Salinity distributions at level 4 (250 m) for runs 132 (left), 120 (center), 138 (right): $d > 1$ (<1) yields a more (less) saline subtropical gyre and less (more) saline subpolar gyre relative to the standard run: c.i. = 0.1. (b) Salinity distributions at level 12 (3250 m) for the same model runs. Note the rotation of deep isohalines to a more zonal (meridional) direction relative to the standard run 120 ($d = 1$) for $d > 1$ ($d < 1$): c.i. = 0.005.

possible reason for this feature of the stability field in section 4.

b. *Experiments with $\hat{s} = 1$, variable $\hat{t}$*

The set of model runs 134, 131, and 139, characterized by $\hat{s} = 1$ and values of $\hat{t}$ from 0.8 to 0.5 (Table 2), was undertaken for two reasons: 1) to explore the conditions under which the "normal" thermohaline cell weakens and a reverse cell forms, and 2) to determine whether model solutions depend mainly on the value of d or whether they are sensitive to the separate values of $\hat{s}$ and $\hat{t}$ by which that value of d is achieved.

The meridional streamfunction sections (Fig. 7) contain much of the information pertinent to both questions. Although there is apparently no abrupt transition between flow regimes, the rate of decrease of transport of the "normal" meridional thermohaline cell is certainly not linear with d: 60% of the decrease of the "normal" cell occurs by $d = 1.25$. The reverse cell forms near a value of $d = 1.5$. The streamfunction fields shown here for run 139 ($d = 2 = 1/0.5$) are very like those shown in Fig. 3 for run 132 ($d = 2 = 2/1$), indicating that the main dynamical effects are pre-

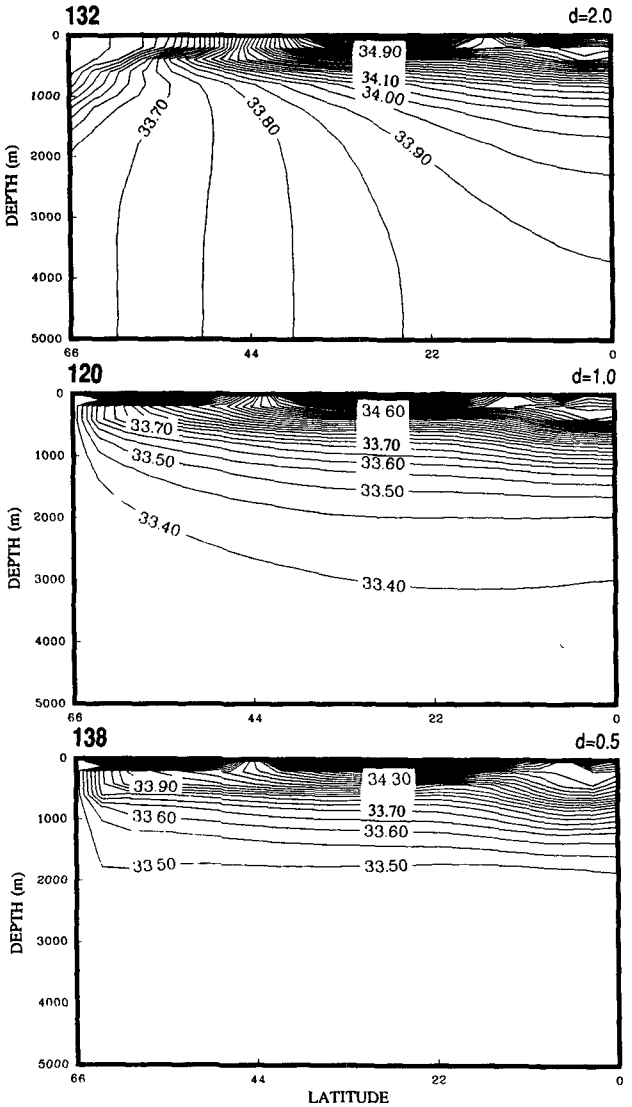

FIG. 5. Sections of S as a function of latitude at 30° longitude for runs 132 (top), 120 (center), 138 (bottom). With $d \leq 1$ the deep salinity field is very homogeneous, while $d > 1$ produces large meridional gradients of S and a salinity minimum near 1000 m in the subpolar gyre.

dominantly a function of d rather than how d is attained through specific values of $\hat{s}$ and $\hat{t}$. The model results are not quantitatively identical (for example, the "normal" thermohaline cell has a maximum transport of 1 Sv (Sv $\equiv 10^6$ m^3 s^{-1}) in run 139, compared with 2 Sv in run 132), but such differences as do occur seem relatively minor compared with the differences between model runs with $d = 1$ and $d = 2$.

The other model diagnostics for these experiments with $d = 1.25$, 1.5, and 2.0 show features that support the idea of an orderly progression between features characteristic of the model with $d = 1$ to those described in the previous section for $d = 2$. On the upper ocean level 4 (not shown), the subtropical gyre becomes more saline, the subpolar gyre very slightly fresher. On the deep-ocean level 12 (not shown), isohalines rotate progressively to near-zonal orientation, and both mean S and the meridional gradient of S increase as the deep subtropical gyre becomes cutoff from the high-latitude freshwater source. As seen in Fig. 8, a distinct subpolar salinity minimum forms near 1000-m depth by $d = 1.5$ and increases in amplitude and equatorward penetration with increase in d. The distribution of vertical density gradient (Fig. 9) shows the only major difference between the two $d = 2$ runs; instead of a smooth

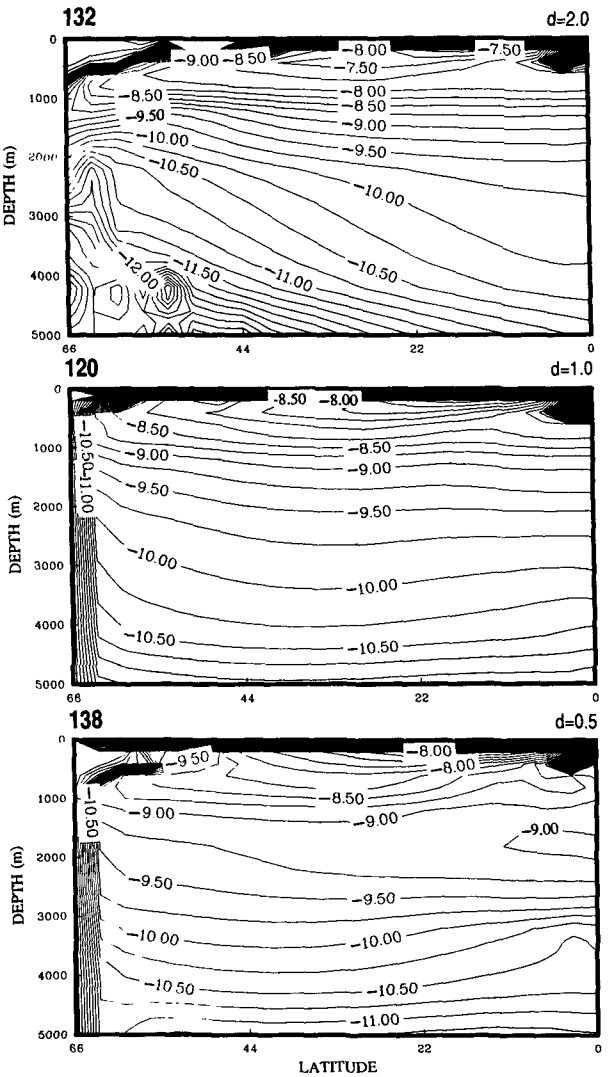

FIG. 6. Sections of $\log(-\rho_z/\rho_0)$ versus latitude for runs 132, 120, and 138. Lowered deep-water stability along the northern boundary in run 132 is a possible effect of maintaining a constant value of d despite evolution of water column T–S structure (for discussion, see section 3d).

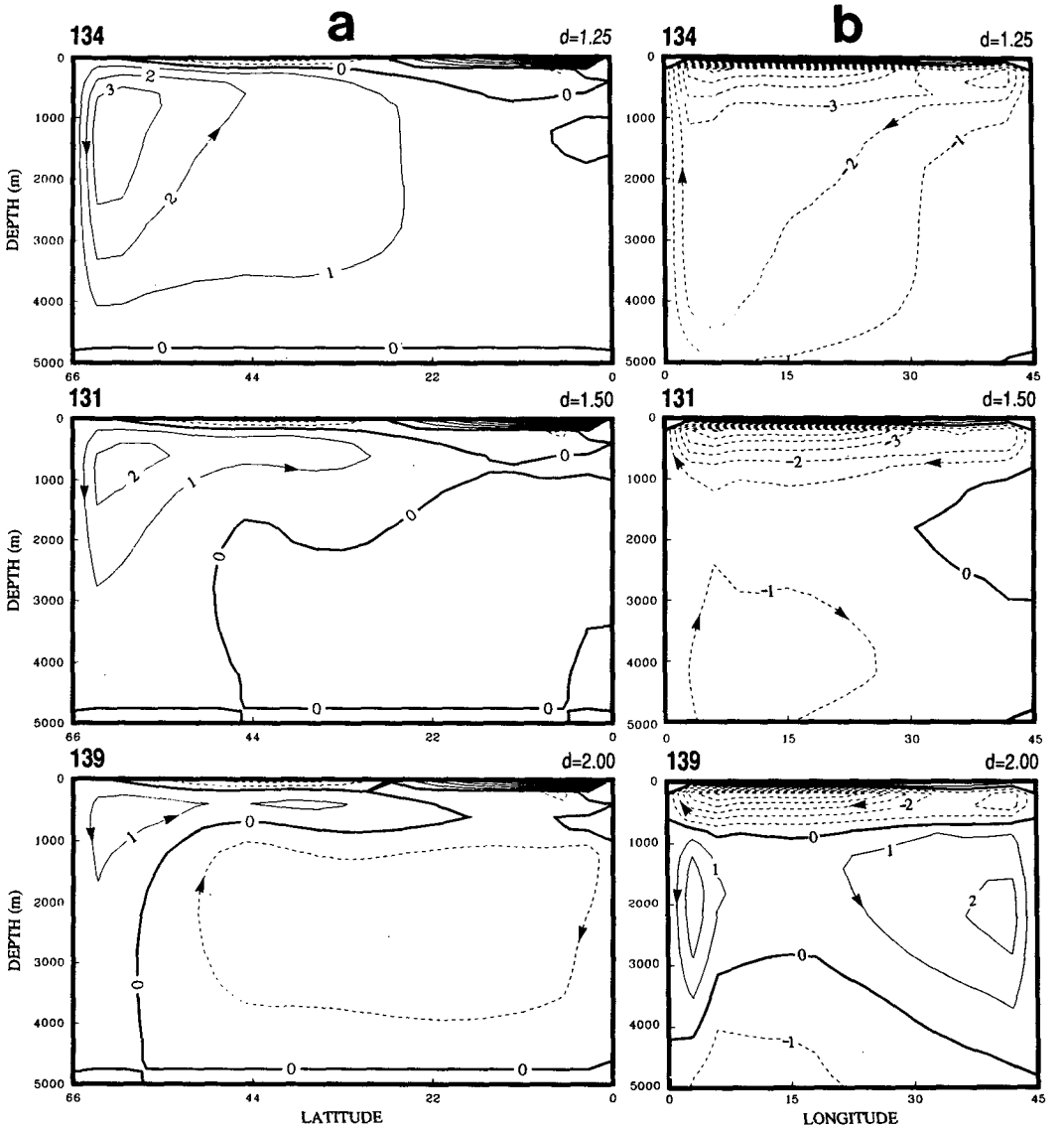

FIG. 7. (a) Meridional and (b) zonal overturning streamfunctions for runs with $\hat{s} = 1$ and varying d ($\hat{t}$). Upper panels: run 134, $d = 1.25$; middle panels: run 131, $d = 1.5$; lower panels: run 139, $d = 2.0$ (c.i. = 1 Sv). Comparison of run 134 with run 120 (Fig. 3, middle) shows that $d = 1.25$ has reduced transport of the normal thermohaline cell by 60%. Comparison of run 139 with run 132 (Fig. 3, upper) shows that the dynamic effect is predominantly associated with the value of d, rather than the specific $\hat{s}$ and $\hat{t}$ values by which it is achieved.

field tending to low values toward the northern boundary (run 132, Fig. 6), run 139 produces a slight stability maximum at ~4000 m in the deep subtropical and equatorial regions.

c. *Experiments with constant D_0*

The preceding sections have described changes in circulation and property distributions that occur when the vertical eddy diffusivities for heat and salt are assumed to have a functional dependence on stratification as $D_0 = a_0 N^{-1}$, with diffusivity ratio $d = D_S/D_T \neq 1$. In this section, we describe two runs that were made with a constant underlying diffusivity $D_0 = 0.3$ cm^2 s^{-1} in order to demonstrate that the major results reported thus far are not associated merely with use of a stratification-dependent diffusivity. We will not dwell on differences between model runs with constant or stratification-dependent diffusivities at $d = 1$, as that ground has been covered in CHG: Here we merely compare two experiments with $D_0 = 0.3$ cm^2 s^{-1} and values of $d = 1$ (run 112) and $d = 2$ (run 113). As

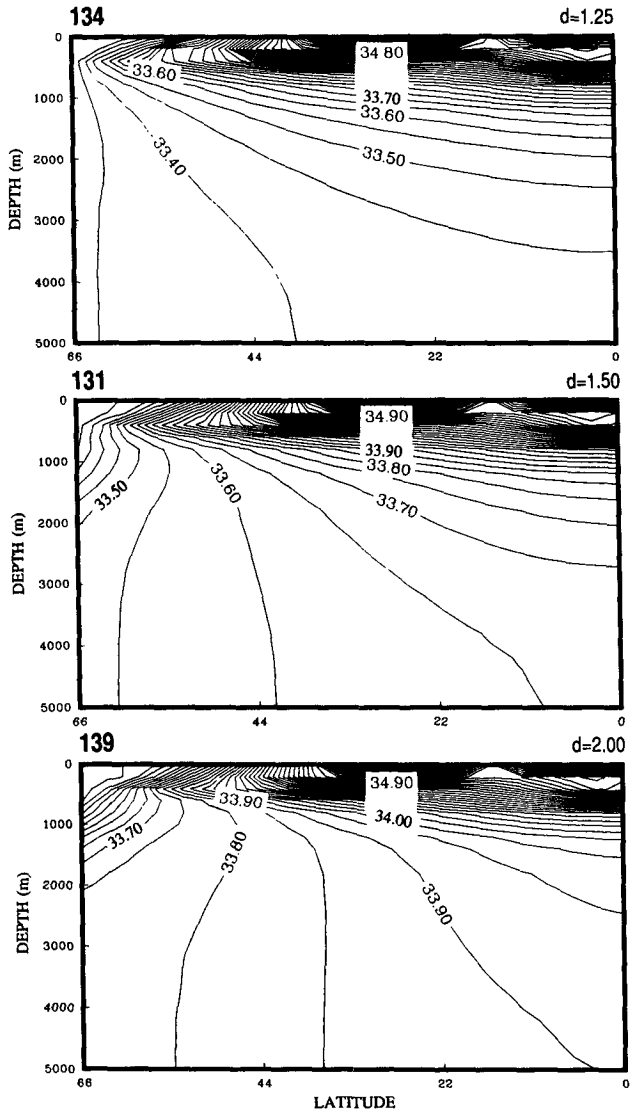

FIG. 8. Sections of S as a function of latitude for runs 134, 131, and 139. The magnitude and extent of a salinity minimum beneath the subpolar gyre increase as d increases.

seen from Table 2, the value $d = 2$ is obtained from $\hat{s} = 2, \hat{t} = 1$, so results from run 113 should be compared with those from run 132 (although from the results of subsection 3b the same qualitative results are obtained with $\hat{s} = 1, \hat{t} = 0.5$, run 139).

With $D_0 = 0.3$ cm^2 s^{-1}, the mass transport streamfunctions, seen in Fig. 10, exhibit the same qualitative changes between the $d = 1$ and $d = 2$ cases, as were seen (Fig. 3) with $D_0 = a_0 N^{-1}$. The normal thermohaline cell of the meridional streamfunction, observed with $d = 1$, is severely reduced in magnitude and confined to the upper ocean with $d = 2$. Replacing it at depths below 1000 m is a reverse cell, similar (although stronger in magnitude and larger in extent) to that observed in run 132. The zonal streamfunction again evolves from a normal cell, sinking over most of the interior and upwelling along the western boundary, to a surface-intensified normal cell. In this case the zonal circulation does not actually reverse at middepth, as it does in run 132, but there is a middepth minimum in zonal transport near 1000 m.

Plan distributions of S at model levels 4 and 12 are shown in Fig. 11. Again, at level 4 the run (113) with higher d has a more saline subtropical gyre (see for example the increased extent of the 35.1 isohaline) and

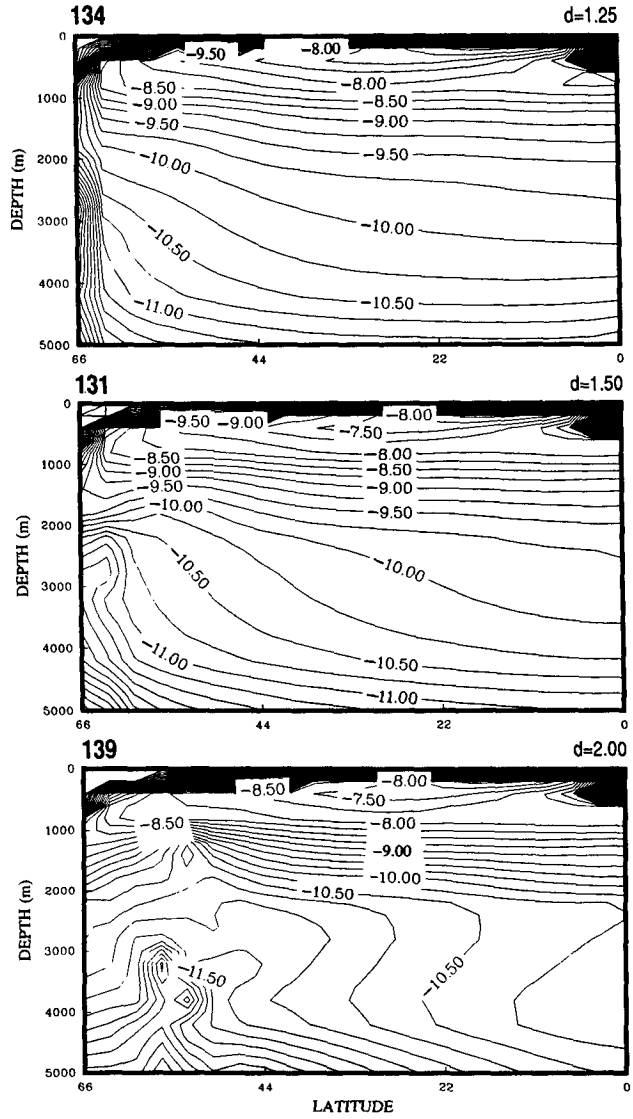

FIG. 9. Distributions of $\log(-\rho_z/\rho_0)$ as a function of latitude for runs 134, 131, and 139. The weak stability maximum near 4000 m in the subtropical gyre of run 139 is the only feature in which the two $d = 2$ experiments (139 and 132) differ substantially.

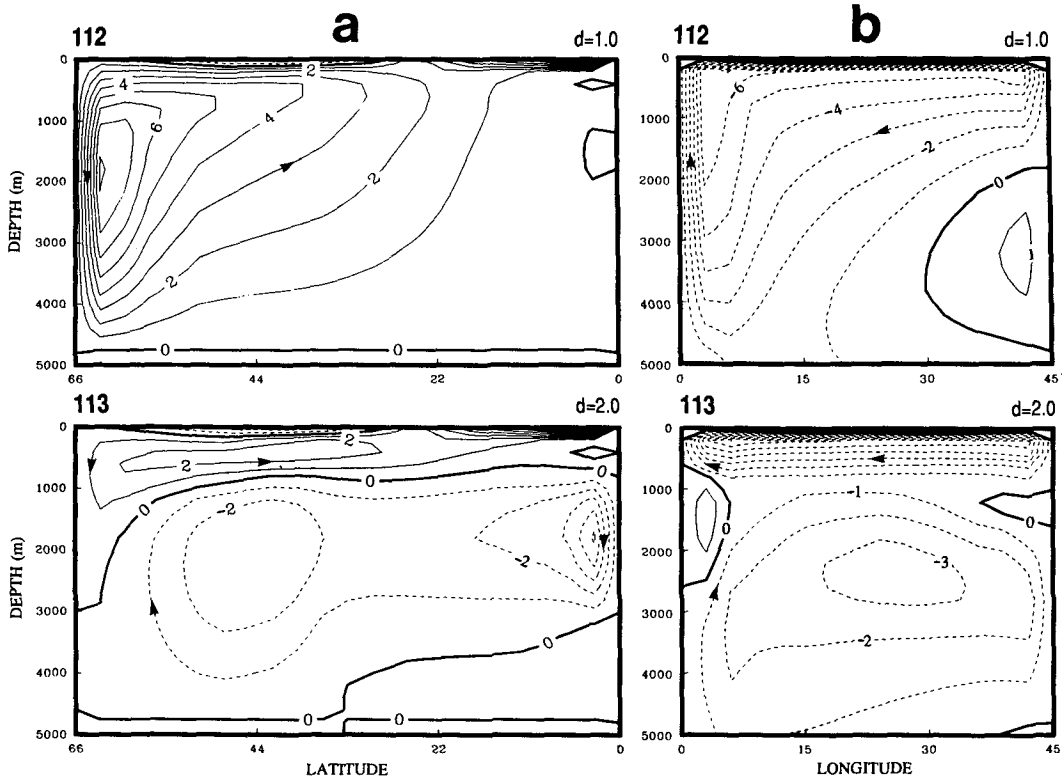

FIG. 10. (a) Meridional and (b) zonal overturning streamfunctions for two runs with $D_0 = 0.3$ cm^2 s^{-1}, $\hat{t} = 1$ but different values of d: $d = 1$ (run 112) and $d = 2$ (run 113). Although different in quantitative detail, this pair of experiments shows the same qualitative differences as the pair of experiments (120 and 132) run with $D_0 = a_0 N^{-1}$.

a slight suggestion of a fresher subpolar gyre. At level 12, run 112 has almost uniform S (too uniform deep-water properties are a commonly known failing of the GFDL model run with constant diffusivity), while run 113, like run 132, shows the nearly zonal isohalines associated with both the larger value of D_S and the isolation of the deep ocean from advection from the surface.

Sections of S as a function of latitude (Fig. 12) show how $d = 2$ is again associated with the existence of a salinity minimum originating near 1000 m in the subpolar gyre. Run 113 has the most intense $S_{\min}$ observed in all the model runs: the minimum extends well into the subtropical gyre, descending to nearly 2000-m depth by ~30°N latitude. The extent of $S_{\min}$ in this experiment is sufficient in that it appears in the section of S versus longitude, hugging the western boundary at approximately the depth of the minimum in zonal streamfunction.

The preceding comparisons of runs 112 and 113 indicate that, although quantitative differences exist, experiments with different d values exhibit very similar qualitative changes, independent of two very different choices of the underlying diffusivity function D_0 (that these *are* very different choices can be seen by reference to Fig. 2 of CHG, which contours $a_0 N^{-1}$ for the equivalent of our run 120). Thus, we feel comfortable in concluding that similar effects will be observed in any runs of the GFDL model carried out with $d \neq 1$.

d. Some consequences of constant diffusivity ratio

The choice of a constant diffusivity ratio $d = D_S/D_T$ seemed a logical first step in the exploration of effects of differing diffusivities for temperature and salinity. However, values of d greater or less than 1 are actually associated with different physical processes, which should turn on (with varying strength) dependent upon the local vertical gradients of T and S. Maintenance of a constant ratio of diffusivities, independent of the gradient distributions that actually evolve in the model runs, has various consequences, which we now explore.

The model gradient distributions are exhibited in the form of a Turner angle Tu, as shown in Fig. 13. Ruddick (1983) defined the Turner angle as the four-quadrant arctangent of R_ρ: we use this definition but subtract 45°, yielding an angle between 0° and 180° for a statically stable water column. Unstable values

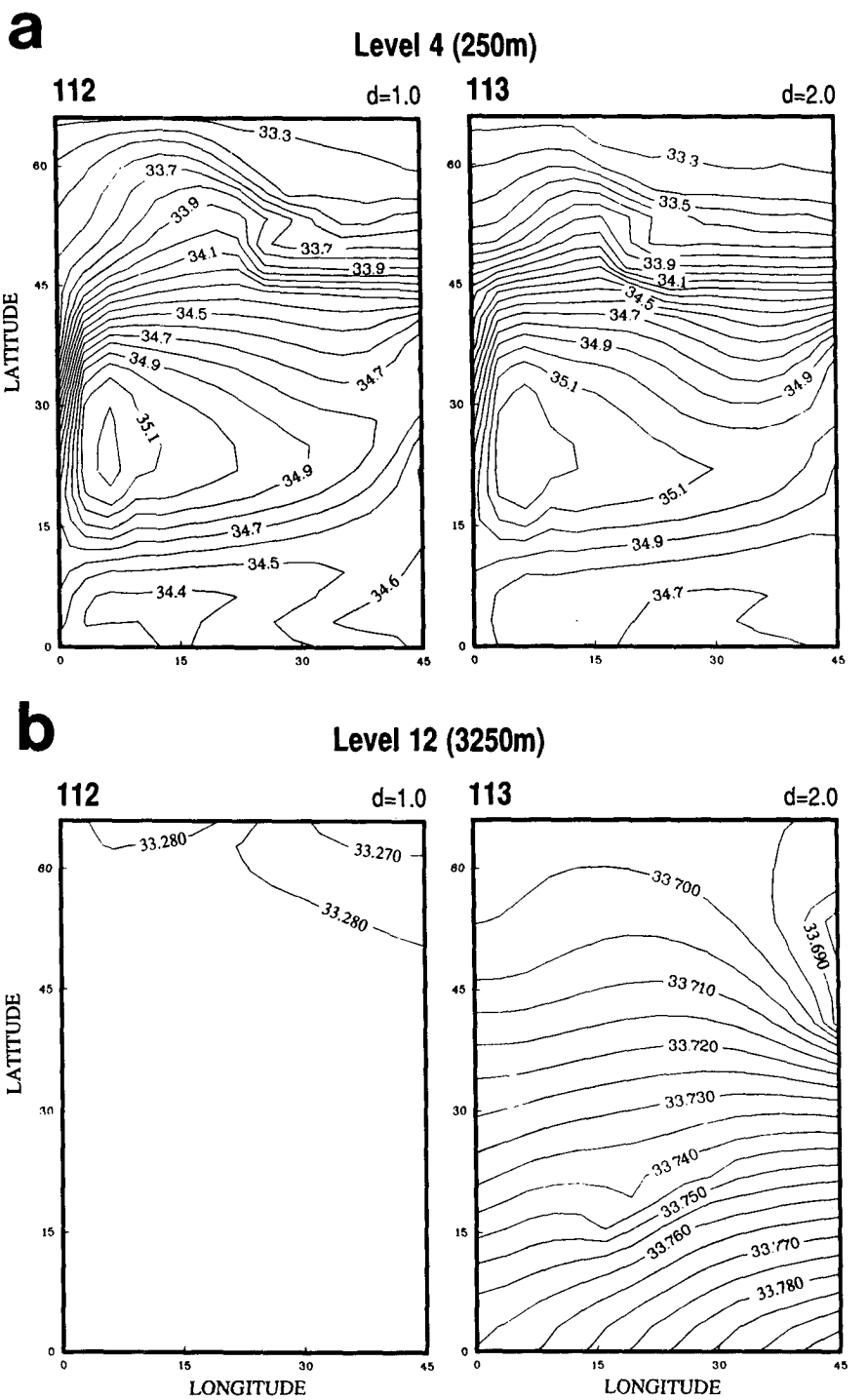

FIG. 11. Salinity at (a) level 4 (250 m, c.i. = 0.1) and (b) level 12 (3250 m, c.i. = 0.005) for runs 112 and 113. With $d = 2$, the deep ocean again exhibits much stronger meridional S gradient and higher S values.

then occupy the ranges 180°–315° and −45°–0° (locating the discontinuity in angle well away from the stable/unstable boundary Tu = 0° for the purposes of contouring). The field of Tu is calculated from the steady-state T and S fields resulting from the model runs, with $T_z = \Delta T/\Delta z$ calculated as the centered dif-

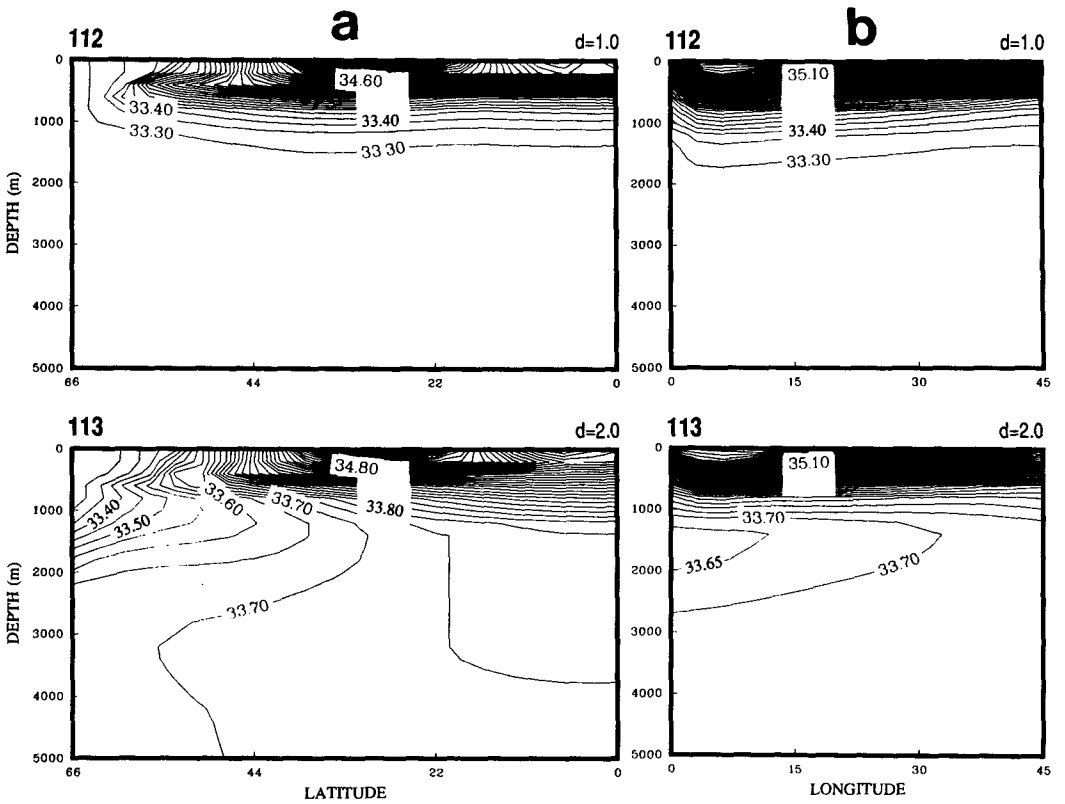

FIG. 12. Sections of salinity as functions of (a) latitude and (b) longitude for runs 112 (upper) and 113 (lower). Despite difference in D_0, $d = 2$ is again characterized by a salinity minimum extending equatorward beneath the subpolar gyre. The minimum is so pronounced in this run that it appears in the longitude section at 30°N as a minimum along the western boundary.

ference of potential temperatures referenced to the mean depth of the layers. Fields of Tu as a function of latitude are contoured in Fig. 14 for the runs discussed in section 3a. The water column properties are unstable to salt fingering ($d > 1$) for $0° < \text{Tu} < 45°$ (light solid contours), both statically and double diffusively stable, but possibly subject to differential diffusion ($d < 1$), for $45° \leq \text{Tu} \leq 135°$ (heavy solid contours), unstable to the layering type of double diffusion ($d < 1$) for $135° < \text{Tu} < 180°$ (dashed contours), and statically unstable for all other values of Tu (dotted contours). As seen in Fig. 14, Tu has very little structure in the standard run 120. Even on the large vertical scales used to calculate the model gradients, the water column below ~500 m has $0° < \text{Tu} < 15°$, implying that it is very unstable to salt fingering throughout the domain, yet throughout the domain of this standard model run $D_S = D_T$. When $d \neq 1$, distributions of Tu are markedly changed. In run 138 the increased vertical uniformity of deep salinity leads to an increase in Tu at depths below 1000 m. In run 132 the presence of the salinity minimum near 1000 m leads to $135° < \text{Tu} < 180°$ at depths below $S_{\min}$ in the subpolar gyre. When, despite the structure in Tu, we continue to impose a constant diffusivity ratio throughout the domain, what effects may we expect? Consider run 132, with $d = 2$, as an example. In the deep subtropical gyre, values of Tu are consistent with salt fingering and, hence, with the imposed relative magnitudes of D_S and D_T. However, below the subpolar $S_{\min}$ (which, although not shown, is also a $T_{\min}$) we now have a water column in which colder, fresher water lies above warmer, saltier water; a case in which we might expect $d < 1$. Nevertheless, continuing to impose $d > 1$ in this region causes a (stabilizing) salinity gradient to diffuse away faster than a (destabilizing) temperature gradient. Thus, the diffusive tendency in the deep subpolar gyre should be toward lower S_z and ρ_z in run 132 where $135° < \text{Tu} < 180°$ than in run 120 where $0 < \text{Tu} < 15°$. Referring back to Fig. 6, we recall that this region does indeed show a substantial decrease in deep water column stability in the subpolar gyre of run 132, compared to run 120. With the evidence (Fig. 3) of much reduced vertical advective fields at depth in run 132, the decrease in stability may be a direct result of maintaining the "wrong" diffusivity ratio.

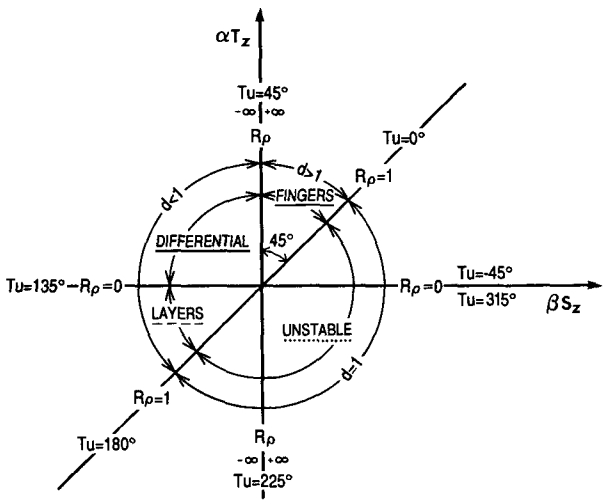

FIG. 13. Definition diagram for the Turner angle Tu used as a measure of type of water column stability. For the salt-fingering instability in $0° < \mathrm{Tu} < 45°$ we may expect $d \equiv D_S/D_T > 1$, while for $45° \leq \mathrm{Tu} < 135°$ we might expect $d < 1$, either as a result of the double-diffusive layering instability or of differential diffusion (for further details, see text). In contour plots of Tu, the various diffusive regimes are contoured with the line type used under the regime labels in this figure.

e. *Model runs with d dependent on local property gradients*

From the preceding section, it is clear that model runs with $d > 1$ develop areas in which local T and S gradients are incompatible with the imposed constant value of d. To move beyond this stage of parameterization requires a diffusivity ratio that depends upon local property gradients that develop in the model run. Ideally, such a variable diffusivity ratio should depend not only on the signs of the mean vertical gradients of T and S but also on their magnitudes. In reality we are not yet able to specify such detailed differential flux parameterizations, even for the salt-fingering mechanism, which has been most actively investigated in the ocean, much less the diffusive layering instability or the differential diffusion mechanism. However, as a first step toward a more realistic implementation of variable diffusivity ratio, we have carried out two additional runs of the present model, using different values of constant d depending upon the sign of computed S_z at each model step, as summarized in Table 3. In regions of the model where $\rho_z < 0$ (static stability), $d = 2$ where salt fingering is possible ($S_z > 0$), but $d = 1$ (run 135) or $d = 0.5$ (run 136) where salt fingering is not possible ($S_z < 0$). Where $\rho_z > 0$ (static instability), $D_S = D_T = 10^4$ cm^2 s^{-1}, as before. This simplified implementation of variable diffusivity ratio is equivalent to assigning d on the basis of the ranges of Tu given in Table 3, but avoids the need to compute Tu at each model point at each time step. In run 136, the value of $d = 0.5$ may be imagined as due to differential diffusion or, if the local temperature gradient is suitable, to diffusive layering.

The meridional and zonal overturning streamfunction fields for these two runs are shown in Fig. 15, compared with run 132 in which $d = \hat{s}/\hat{t} = 2/1$ is kept fixed throughout the domain. The flow fields are similar among the three runs, the main difference being in zonal streamfunction where the middepth reversed flow cell of run 132 weakens to a minimum in runs 135 and 136.

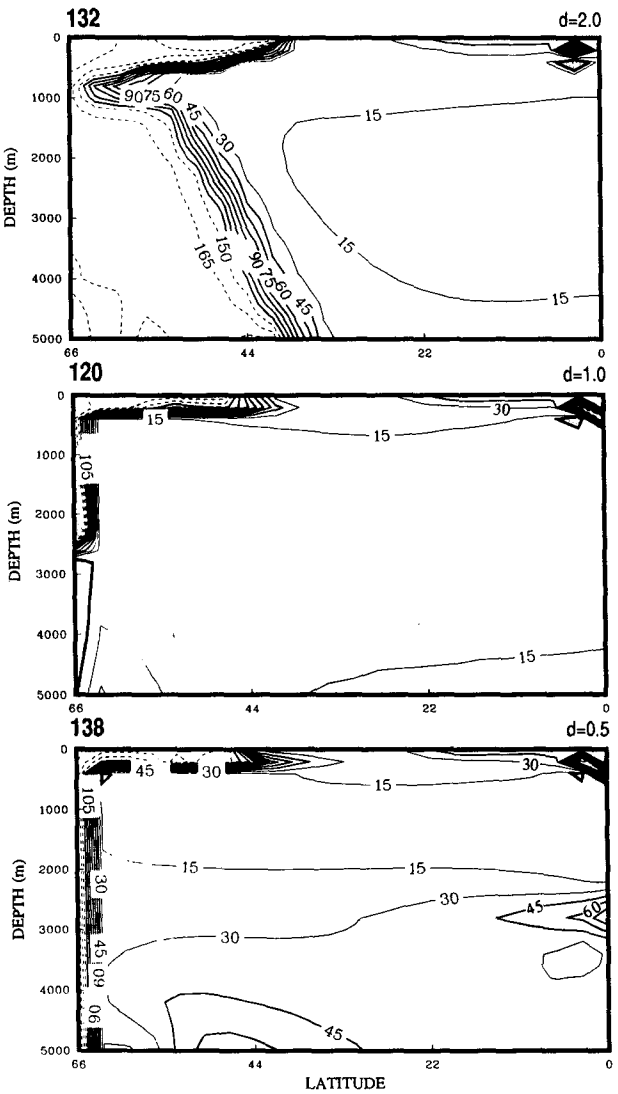

FIG. 14. Contour plots (c.i. = 15°) of Turner angle Tu for runs 132 (top), 120 (middle), and 138 (bottom). The standard run, run 120, is characterized by very uniform values of $0 < \mathrm{Tu} < 15°$ nearly everywhere below ~1000-m depth, suggesting a strong tendency to the salt-fingering instability. With $d < 1$, Tu increases below ~1000-m in depth (due to $S_z \to 0$), while $d > 1$ has values of $135° < \mathrm{Tu} < 180°$ below the observed salinity minimum (Fig. 5).

TABLE 3. Vertical diffusivity parameters for model runs in which diffusivity ratio $d \equiv D_S/D_T$ depends upon local property gradients (for definition of Turner angle Tu, see Fig. 13). $D_T = \hat{t}D_0$, $D_S = \hat{s}D_0$, hence, $d = \hat{s}/\hat{t}$; $D_0 = a_0N^{-1}$.

Run	d	$\hat{s}$	$\hat{t}$	Condition
135	2	2	1	$S_z > 0$; $0° < \text{Tu} < 45°$
	1	1	1	$S_z < 0$; $45° < \text{Tu} < 225°$
136	2	2	1	$S_z > 0$; $0° < \text{Tu} < 45°$
	0.5	0.5	1	$S_z < 0$; $45° < \text{Tu} < 225°$

Unlike the streamfunction fields, however, distributions of T and S differ substantially when d is no longer held constant (Fig. 16). Run 135 develops a high-latitude salinity (and associated temperature) minimum that is much more pronounced than in run 132. Note also that deep S and T values are higher than those in run 132. In run 136, the salinity minimum has weakened and moved deeper in the water column, and deep salinity has increased still further. Most significantly, the high-latitude salinity minimum is no longer associated with a temperature minimum, increasing the resemblance of the model property fields to those observed in the ocean. It seems likely that judicious tuning of the value of d in the model regions where $S_z < 0$ (i.e., beneath the $S_{\min}$) could produce both a temperature field that is monotonic with depth and a salinity field with $S_{\min}$ of observed magnitude and depth. The point is not that such tuning should be carried out but that water mass properties of the steady-state model solution are apparently extremely sensitive to implementation of different diffusivity ratios as a function of local properties, as these evolve during the model run.

Deep ocean stability is also very sensitive to variable d, as seen in Fig. 17. Like run 132, run 135 continues to exhibit low values of ρ_z toward the northern boundary. Run 136 on the contrary shows no sign of this northern boundary effect: low stabilities are found only in a bottom boundary layer, and the stratification in the deep interior (1–4 km) is the strongest observed in the entire set of model runs.

4. Effect of vertical diffusivity parameterization on factors of climatic importance

We now examine the effect of d on the aspects of a model ocean that are of major importance to long timescale climate modeling, the meridional transports of heat and salt (or alternatively, freshwater), and the mass transport and morphology of the normal thermohaline cell.

Meridional transports of heat and salt by the thermohaline circulation are the major pathway of interaction between ocean and atmosphere on the time scales associated with climate change, and their central importance has long been recognized. Figure 18 summarizes the effects of d and D_0 on these fluxes. At midlatitudes the major change in heat flux (Fig. 18a) is associated with difference in D_0. For example, at 30°N the heat flux obtained with $D_0 = 0.3$ cm^2 s^{-1}, $d = 1$ (run 112, filled squares) is twice that obtained with $D_0 = a_0N^{-1}$, $d = 1$ (run 120, filled circles). Because the relation $D_0 = a_0N^{-1}$ produces upper-ocean values that are less than 0.3 cm^2 s^{-1}, this is consistent with both the result of Bryan (1987) that heat flux decreases with decreasing (constant) diffusivity, and the result of CHG, who found that the heat flux was most strongly dependent on diffusivity values in the upper ocean. At these latitudes, further change of heat flux with d is relatively small (see the range about the curve obtained with $D_0 = a_0N^{-1}$, $d = 1$; open symbols). However, this situation reverses at latitudes higher than ~50°: here variation of D_0 has little effect, while variation of d over the chosen range produces heat flux values that can be 50% lower (runs 139, 132; $d = 2$) or higher (run 138; $d = 0.5$) than the standard (run 120). In addition, the slope (divergence) of the heat flux curve varies with d at these high latitudes. Because divergences of ocean fluxes imply ocean–atmosphere coupling this aspect of variation with d may be of greater importance for climate studies than the changes in magnitude.

Essentially, the same behavior is found in the model salt fluxes (Fig. 18b). The magnitude of the salt flux at low- and midlatitudes is mostly influenced by D_0 (although the dominance of this effect over that of d is not as pronounced as it is for the heat fluxes), while variation in salt flux and flux divergence at latitudes higher than ~50° is predominantly caused by d.

While model heat and salt fluxes have a direct connection with the overlying atmosphere in any coupled GCM, a less direct effect involves the potential of the ocean as a sink of CO_2 and other greenhouse gases. It is believed that part of the action of the ocean sink involves the process by which dissolved gases are removed from contact with the atmosphere by export to the deep ocean, at least over the several-hundred-year time scale believed typical of the present thermohaline circulation. In this connection, it is clear that the effectiveness of model oceans in sequestering greenhouse gases depends not only on the magnitude of mass flux in the normal thermohaline cell but also on its morphology; more particularly the volume it occupies. Reduced to the simplicity of a filling box, the renewal time $T_r = V/F$ after which we may expect to see water that sank at high latitudes back at the surface is dependent not only on F, the volume transport, but also on V, the volume that must be "filled." Rough calculations of T_r for each run can be based on the maximum value of F in the normal meridional cell, together with an estimate of the volume of the cell. The normal cell already occupies almost all of the model volume

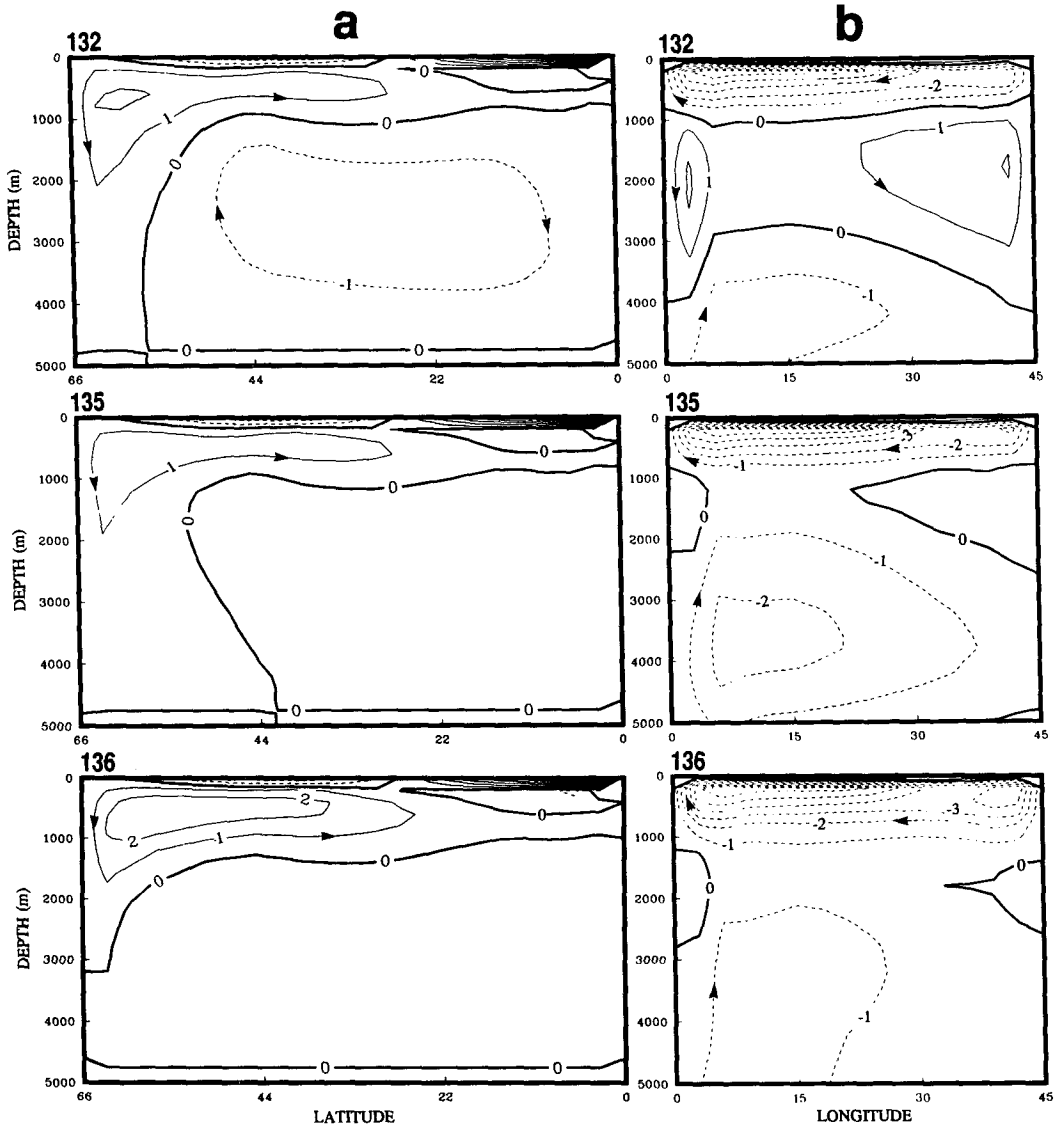

FIG. 15. (a) Meridional and (b) zonal overturning streamfunctions for model runs incorporating a rudimentary dependence of d on local stratification: if $S_z > 0$, $d = 2$, while if $S_z < 0$, $d = 2$ (run 132, top), $d = 1$ (run 135, middle), or $d = 0.5$ (run 136, bottom). See Table 3 and section 3e for details.

in the reference $d = 1$ case (run 120, Fig. 3): using the box geometry, a rough estimate of $T_r \approx 500$ years is obtained. When $d = 0.5$ (run 138), the increased transport occupies the same volume, so $T_r \approx 340$ years is 33% shorter than the standard model. When $d = 2$ (run 132), we estimate the volume of the reduced normal cell as the entire model volume of latitudes greater than 55°, plus the upper kilometer of the box at lower latitudes. This smaller volume (approximately 30% of the total box volume) partly offsets the dramatic reduction in flux, so the resulting renewal time $T_r \approx 610$ years is only 20% greater than the standard case. The present results suggest that the potential of the ocean as a sink for anthropogenic CO_2 is most seriously (adversely) affected by $d < 1$.

5. Interpretive discussion and conclusions

The GFDL ocean model used in this work incorporates fully nonlinear dynamics and a somewhat simplified but nevertheless nonlinear equation of state for seawater (Bryan and Cox 1972). In such a complex system it is difficult to isolate and understand the mechanism(s) by which change in a particular model parameter causes the changes observed in model results. Consequently, we often attempt to assess at least

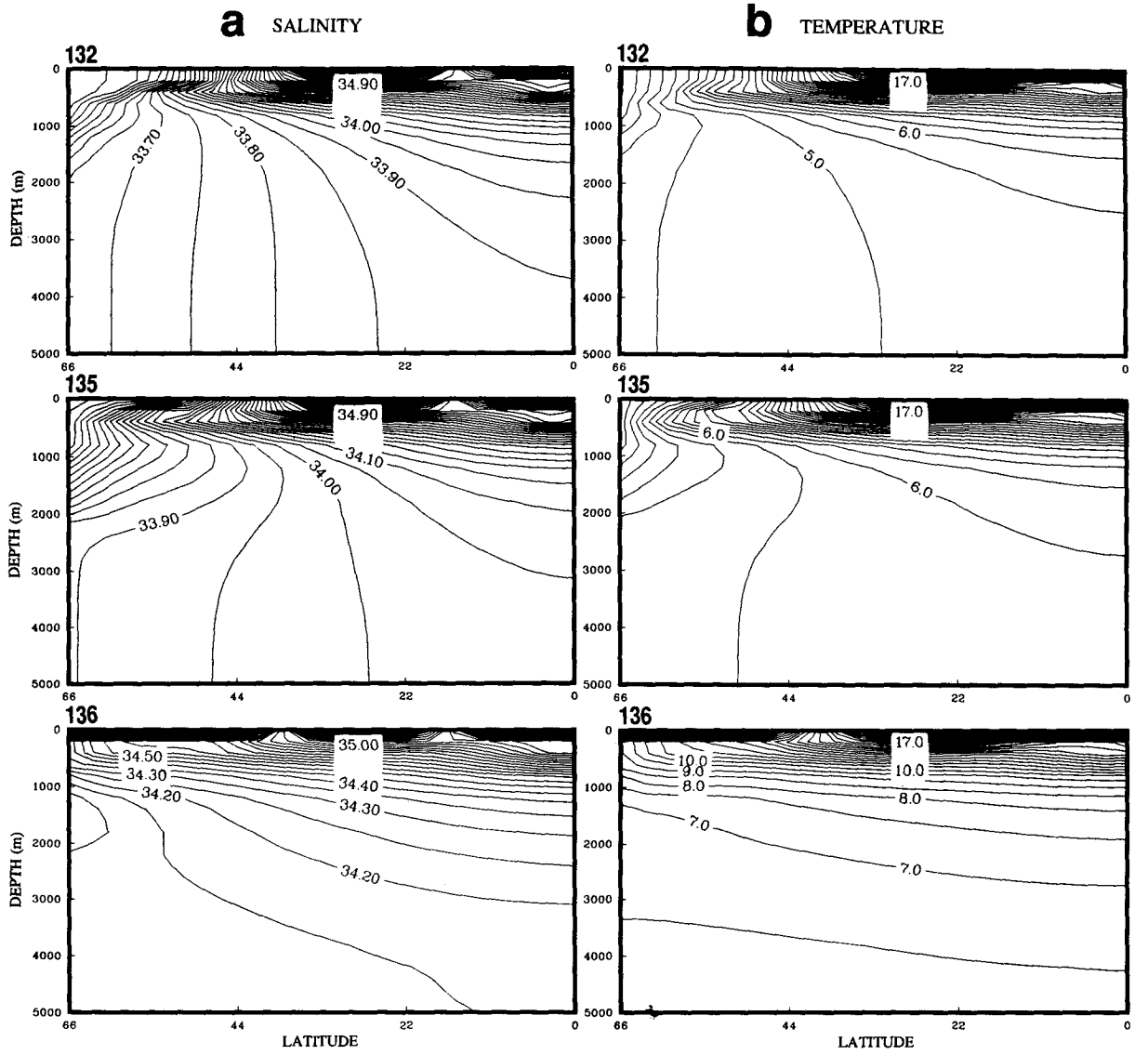

FIG. 16. (a) Salinity and (b) temperature sections with latitude for model runs incorporating rudimentary dependence of d on local stratification (see caption to Fig. 15). Major changes are observed in model water mass structure.

the qualitative sense of such changes using very simplified balances.

As a framework for assessing the present numerical results, let us consider the effect of $d \neq 1$ on the hypothesis that a steady-state density field is maintained by a (linear) balance between vertical advection of density and vertical diffusion of density, with effective density diffusivity D. This balance,

$$w\rho_z = (D\rho_z)_z, \qquad (2)$$

(or its simpler equivalent with D = constant) has a long history of use in oceanographic modeling (Robinson and Stommel 1959; Munk 1966). Although it has fallen into disfavor as a theory for the main pycnocline, now widely believed to be of predominantly quasi-horizontal advective origin, it may yet serve in intermediate and deep waters, where Colin de Verdière (1989) finds such a balance in a recent model. Since the dynamical differences that we observe among the present set of model runs have their origins in differences in the (effective) vertical diffusive term in the density equation, we may obtain some feel for the direction of such effects using this simple balance.

What then is an equivalent diffusivity for density in numerical models having $d \neq 1$? Consider the conservation equations for (potential) temperature T and sa-

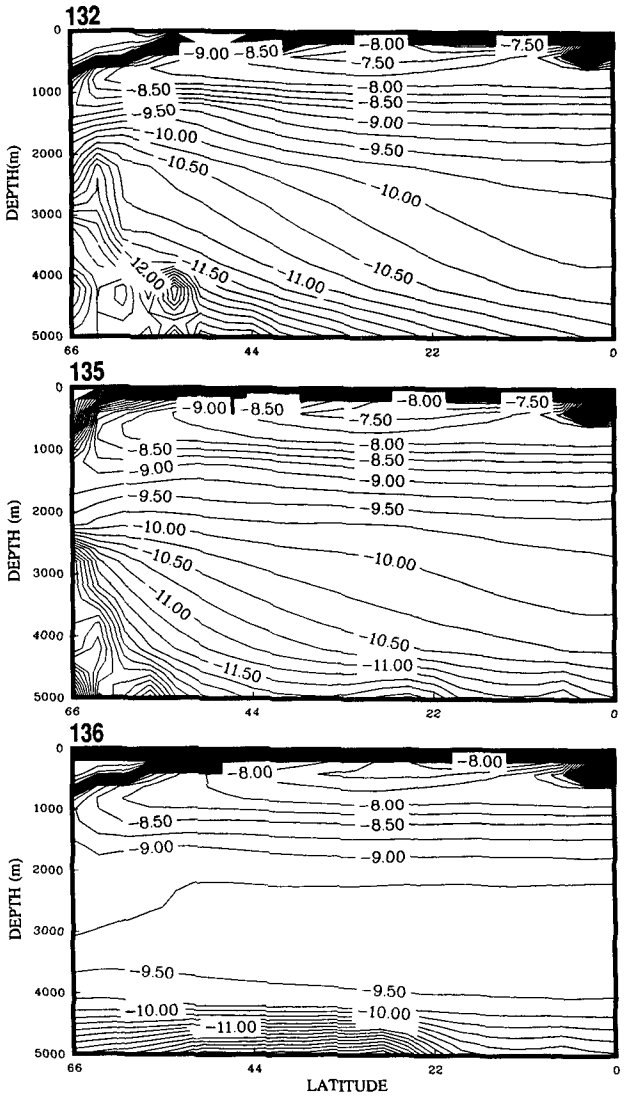

FIG. 17. Distribution of $\log(-\rho_z/\rho_0)$ as a function of latitude for model runs incorporating rudimentary dependence of d on local stratification (see caption to Fig. 15).

linity S in the (geographic) coordinate system used by the model

$$T_t + \mathbf{V}\cdot\nabla_h T + wT_z = (D_T T_z)_z + \cdots \quad (3)$$

$$S_t + \mathbf{V}\cdot\nabla_h S + wS_z = (D_S S_z)_z + \cdots, \quad (4)$$

where the ellipses denote horizontal diffusion and forcing terms. For simplicity, we assume a linear equation of state $\rho = \rho_0(1 - \alpha T + \beta S)$ so that $\rho_0^{-1}\rho_z = -\alpha T_z + \beta S_z$, etc. Multiplying (3) by $-\rho_0\alpha$, (4) by $\rho_0\beta$ and adding yields the steady-state density equation

$$\mathbf{V}\cdot\nabla_h\rho + w\rho_z = [(-D_T\alpha T_z + D_S\beta S_z)_z \equiv (D\rho_z)_z] + \cdots,$$

where D, an equivalent diffusivity for density, is defined as

$$D = D_T\left(\frac{R_\rho - d}{R_\rho - 1}\right) = \hat{t}D_0\left(\frac{R_\rho - d}{R_\rho - 1}\right). \quad (5)$$

In this form it is clear that D depends not only on diffusive parameters (D_0, $\hat{t}$, d) that are set externally but also on the field of R_ρ, which is internally determined by the model solution. Note that where $1 < R_\rho < d$ or $d < R_\rho < 1$, D becomes negative, corresponding to countergradient density flux, even though the individual fluxes of heat and salt are both in the normal downgradient direction. Through its dependence on R_ρ (and possibly D_0), D will be a spatially complicated field, so it is not possible to calculate "the" value of D for a particular model run, even at steady state. However, to give some idea of a range of D covered by the

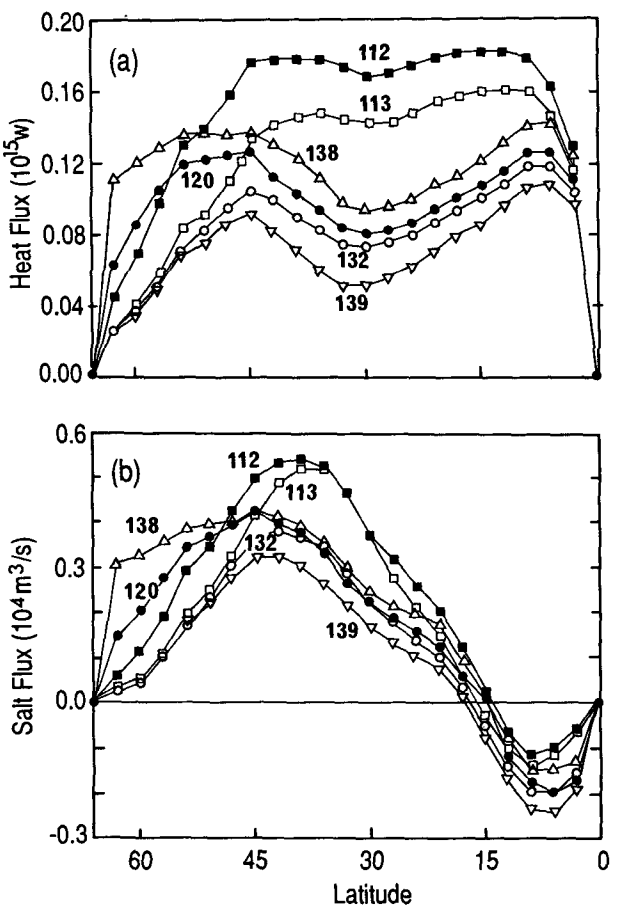

FIG. 18. Meridional heat flux (a) and salt flux (b) as functions of latitude for the runs listed in Table 2. At latitudes less than ~45°N, the major effect on heat and salt fluxes is that of D_0 [compare runs 112 (filled box, $D_0 = 0.3$ cm^2 s^{-1}) and 120 (filled circle, $D_0 = a_0N^{-1}$), both $\hat{s} = \hat{t} = 1$]. At higher latitudes the value of d has the major effect on fluxes.

suite of numerical experiments, the last column of Table 2 lists $D_{1.5}/D_0$, the value of D calculated for $R_\rho = 1.5$ (a value typical of intermediate depths of the subtropical gyre in all runs) and normalized by D_0.

The standard run 120 [carried out with effective diffusivity of density $D = \hat{t}D_0(R_\rho - d)/(R_\rho - 1) = a_0N^{-1}$ since $\hat{t} = d = 1$ and $D_0 = a_0N^{-1}$] develops a steady-state thermohaline field with $R_\rho < 2$, or equivalently Tu $\lesssim 20°$, over most of the interior below $\sim$1000 m (Fig. 14), values suggesting that salt fingering should be active. Assuming that the density field of run 120 is in a vertical diffusive–advective balance with $d = 1$, consider the effect of turning on diffusion with $d = 2$ ($\hat{t} = 1$). Now

$$D = \hat{t}D_0\left[\frac{R_\rho - d}{R_\rho - 1}\right] < 0, \quad \text{since} \quad R_\rho - d < 0$$

over most of the interior. From (2)

$$w = D_z + D\frac{\rho_{zz}}{\rho_z} = D\frac{N_z}{N},$$

where we have used the definition of N^2, Eq. (5) with $D_0 = a_0N^{-1}$, and taken $[(R_\rho - d)/(R_\rho - 1)]_z = 0$ because of the uniformity of R_ρ (Tu) observed in run 120. Since $N_z > 0$ in the intermediate and deep waters, we see that the sign of w is that of D. Thus, $D < 0$, as in the case $d = 2$, $\hat{t} = 1$ of run 132, requires $w < 0$ (downwelling), a reversal of the normal thermohaline flow in the deep interior. Note also that if the underlying diffusivity $D_0 = \text{const}$, rather than a_0N^{-1}, the expression for w becomes

$$w = \frac{2DN_z}{N},$$

which is *twice* that obtained when $D = a_0N^{-1}$. This suggests that the reversed flow of run 113 should be stronger than that of run 120, as is indeed observed.

The preceding discussion perhaps belabors an obvious point. If a model density field is in vertical advective/diffusive balance under a particular magnitude of diffusive density flux, then increasing or decreasing the diffusive flux requires an associated increase or decrease in advection. When, as may happen for particular combinations of R_ρ and d, the diffusive density flux actually reverses direction, the balancing advective term must also reverse.

This discussion represents only a tendency that we expect to observe when $d \neq 1$, and details will certainly depend upon the distribution of R_ρ as it evolves away from the very uniform field of run 120. Despite its simplicity however, the assumption that intermediate and deep density fields (at least in subtropical regions) are in a vertical advective/diffusive balance, with an effective diffusivity for density given by Eq. (5), serves rather well in explaining the nature of the major changes in circulation observed in our model runs; both changes with d for constant D_0 (subsections 3a and 3b) and changes with D_0 for constant d (subsection 3c).

This work was a first attempt to explore the sensitivity of coarse-resolution numerical models, of the kind presently used for predictive climate studies, to the usual assumption that the turbulent eddy diffusivities for T and S are identical; hence, $d = D_S/D_T \equiv 1$. We have found certain features of the model results that are extremely sensitive to this assumption, namely, the magnitude and sense of the thermohaline circulation, water mass characteristics, and intermediate- and deep-water stability distributions. Certain integrated model features that are of fundamental importance to the present generation of coupled ocean–atmosphere models used for climate studies appear to be less sensitive. In particular, meridional heat transports at mid-latitudes are less affected by different diffusivities for T and S than by the difference between constant and stability-dependent diffusivities, with their different upper-ocean values. The observed sensitivity to d of heat fluxes and flux divergences at subpolar latitudes may be important, however, since it is at these latitudes that the ocean delivers heat to the atmosphere.

To first order, the time scale over which anthropogenic CO_2 may be sequestered in the deep ocean increases if $d > 1$, although observed decrease in transport of the normal meridional cell (in which water sinks at high latitudes) is at least partially compensated by observed decrease in cell extent. If $d < 1$ however, residence time decreases in roughly inverse proportion to the observed increase in meridional transport, since at $d = 1$ the cell already occupies most of the model volume.

Based on present results, it is the diffusivity *ratio* $d = D_S/D_T$ that largely determines the character of the model solution rather than the particular choice of individual values D_S, D_T by which the value of d is achieved. Further exploration of the two-parameter space (D_S, D_T) would seem advisable.

The observed sensitivity of the GFDL model to relatively minor variation in d raises significant questions for both modeling and microscale observations. With respect to models, we would like to know whether (how) the effects of $d \neq 1$ differ when the domain is global, rather than the single-hemisphere box considered here. The effects of $d \neq 1$ should also be assessed for the box-model oceans that are often coupled to an energy-balance atmospheric model and used to predict climate change (Bretherton et al. 1990). Preliminary results show significant changes to such a coupled model. More fundamentally, we would like to understand the mechanisms by which d affects model characteristics, particularly the subpolar salinity minimum. In this regard, it might be most effective to carry out preliminary work with a model, such as that of Colin de Verdière (1989), which avoids the (possibly unes-

sential) complications of nonlinearity in the momentum balances. The sensitivity of the GFDL model results to d also presents major challenges to the microscale observational community. As remarked earlier, the conditions under which differential diffusion occurs are essentially unknown: this process must be much better understood before it is possible to assess its importance in the ocean. Although much more is known of double diffusive transports, there is little to guide us when both double diffusion and "ordinary" turbulence occur together, as they do in the ocean. How can the naturally occurring processes be better quantified through observational techniques? These questions must be addressed if we are to proceed beyond the simplest differential flux parameterization (constant d) as used in this paper.

Acknowledgments. Dave Ramsden carried out most of the computations reported here, maintaining good cheer in a thicket of diagnostic plots. P. Cummins modified the GFDL code to run different diffusivities for T and S. This work was carried out under ONR Grant N00014-87-J-1262.

REFERENCES

Altman, D. B., and A. E. Gargett, 1987: Differential property transport due to incomplete mixing in a stratified fluid. *Proc. Third Int. Symp. on Stratified Flows.* Pasadena, California Institute of Technology.

Bretherton, F. P., K. Bryan, and J. D. Woods, 1990: Time-dependent greenhouse-gas-induced climate change. *Climate Change: The IPCC Scientific Assessment,* J. T. Houghton, G. J. Jenkins, and J. J. Ephraums, Eds., Cambridge University Press, 364 pp.

Bryan, F., 1987: On the parameter sensitivity of primitive equation ocean general circulation models. *J. Phys. Oceanogr.,* **17,** 970–985.

Bryan, K., 1984: Accelerating the convergence to equilibrium of ocean-climate models. *J. Phys. Oceanogr.,* **14,** 666–673.

——, and M. D. Cox, 1967: A numerical investigation of the oceanic general circulation. *Tellus,* **19,** 54–80.

——, and ——, 1972: An approximate equation of state for numerical models of the ocean circulation. *J. Phys. Oceanogr.,* **2,** 510–514.

——, and J. L. Sarmiento, 1985: Modeling ocean circulation. *Adv. Geophys.,* **28A,** 433–459.

——, S. Manabe, and M. J. Spelman, 1988: Interhemispheric asymmetry in the transient response of a coupled ocean–atmosphere model to a CO_2 forcing. *J. Phys. Oceanogr.,* **18,** 851–867.

Colin de Verdière, A., 1989: On the interaction of wind and buoyancy driven gyres. *J. Mar. Res.,* **47,** 595–633.

Cummins, P. F., G. Holloway, and A. E. Gargett, 1990: Sensitivity of the GFDL ocean general circulation model to a parameterization of vertical diffusion. *J. Phys. Oceanogr.,* **20,** 817–830.

Gargett, A. E., 1984: Vertical eddy diffusivity in the ocean interior. *J. Mar. Res.,* **42,** 359–393.

GEOSECS Atlas, 1981: Vol. 2 (Atlantic) and Vol. 4 (Pacific). Superintendent of Documents, U.S. Govt. Printing Office.

Kunze, E., 1987: Limits on growing, finite-length salt fingers: A Richardson number constraint. *J. Mar. Res.,* **45,** 533–556.

Munk, W. H., 1966: Abyssal recipes. *Deep-Sea Res.,* **13,** 707–730.

Robinson, A., and H. Stommel, 1959: The oceanic thermocline and the associated thermohaline circulation. *Tellus,* **11,** 295–308.

Ruddick, B., 1983: A practical indicator of the stability of the water column to double-diffusive activity. *Deep-Sea Res.,* **30**(10A), 1105–1107.

Schmitt, R. W., Jr., 1979: Flux measurements on salt fingers at an interface. *J. Mar. Res.,* **37,** 419–436.

Turner, J. S., 1965: The coupled turbulent transports of salt and heat across a sharp density interface. *Int. J. Heat Mass Trans.,* **8,** 759–767.

——, 1968: The influence of molecular diffusivity on turbulent entrainment across a density interface. *J. Fluid Mech.,* **33,** 639–656.

——, 1973: *Buoyancy Effects in Fluids.* Cambridge University Press, 367 pp.

Washington, W. M., and G. A. Meehl, 1989: Climate sensitivity due to increased CO_2: Experiments with a coupled atmosphere and ocean general circulation model. *Climate Dyn.,* **4,** 1–38.

Weaver, A. J., and E. S. Sarachik, 1990: On the importance of vertical resolution in ocean general circulation models. *J. Phys. Oceanogr.,* **20,** 600–609.